CHEMISTRY
A EUROPEAN JOURNAL

DOI: 10.1002/chem.200600752

An Efficient Hybrid, Nanostructured, Epoxidation Catalyst: Titanium Silsesquioxane–Polystyrene Copolymer Supported on SBA-15

Lei Zhang,[a] Hendrikus C. L. Abbenhuis,*[b] Gijsbert Gerritsen,[b] Nollaig Ní Bhriain,[b] Pieter C. M. M. Magusin,[b] Brahim Mezari,[b] Wei Han,[b] Rutger A. van Santen,*[b] Qihua Yang,[a] and Can Li*[a]

Abstract: A novel interfacial hybrid epoxidation catalyst was designed with a new immobilization method for homogeneous catalysts by coating an inorganic support with an organic polymer film containing active sites. The titanium silsesquioxane (TiPOSS) complex, which contains a single-site titanium active center, was immobilized successfully by in-situ copolymerization on a mesoporous SBA-15-supported polystyrene polymer. The resulting hybrid materials exhibit attractive textural properties (highly ordered mesostructure, large specific surface area ($>380\ m^2g^{-1}$) and pore volume ($\geqq 0.46\ cm^3g^{-1}$)), and high activity in the epoxidation of alkenes. In the epoxidation of cyclooctene with *tert*-butyl hydrogen peroxide (TBHP), the hybrid catalysts have rate constants comparable with that of their homogeneous counterpart, and can be recycled at least seven times. They can also catalyze the epoxidation of cyclooctene with aqueous H_2O_2 as the oxidant. In two-phase reaction media, the catalysts show much higher activity than their homogeneous counterpart due to the hydrophobic environment around the active centers. They behave as interfacial catalysts due to their multifunctionality, that is, the hydrophobicity of polystyrene and the polyhedral oligomeric silsesquioxanes (POSS), and the hydrophilicity of the silica and the mesoporous structure. Combination of the immobilization of homogeneous catalysts on two conventional supports, inorganic solid and organic polymer, is demonstrated to achieve novel heterogeneous catalytic ensembles with the merits of attractive textural properties, tunable surface properties, and optimized environments around the active sites.

Keywords: epoxidation · mesoporous materials · organic–inorganic hybrid composites · polystyrene · titanium

Introduction

Polyhedral oligomeric silsesquioxanes (POSS) are part of a large family of polycyclic compounds built up through silicon–oxygen bonds. They can have fully or incompletely condensed cage structures.[1,2] As they have a structural resemblance to silica surfaces, incompletely condensed POSS possessing silanol groups have been investigated extensively in the past few years.[3–6] Consequently, metal-containing POSS compounds have been considered as ideal models for mimicking essential features of heterogeneous silica-supported metal catalysts. Numerous elements throughout the periodic table have been incorporated successfully into POSS.[5] Applications are also being developed for the metal–POSS compounds themselves as highly active homogeneous catalysts,[3–6] among which POSS-ligated titanium(IV) complexes (TiPOSS) have proven to be highly active for epoxidation of alkenes.[7–14] There has been considerable research recently on heterogenization of homogeneous catalysts due to the ease of separation and purification of the products and the recovery of the catalysts. Thus, development of active heterogeneous catalysts with predefined active sites by immobilizing metal–POSS compounds on insoluble supports appears promising.

[a] L. Zhang, Prof. Dr. Q. Yang, Prof. Dr. C. Li
State Key Laboratory of Catalysis
Dalian Institute of Chemical Physics
Chinese Academy of Sciences
457 Zhongshan Road, Dalian 116023 (China)
Fax: (+86) 411-8467-4447
E-mail: canli@dicp.ac.cn

[b] Dr. H. C. L. Abbenhuis, Dr. G. Gerritsen, Dr. N. N. Bhriain, Dr. P. C. M. M. Magusin, B. Mezari, W. Han, Prof. Dr. R. A. van Santen
Schuit Institute of Catalysis
Eindhoven University of Technology, PO Box 513
5600 MB Eindhoven (The Netherlands)
Fax: (+31) 40-245-5054
E-mail: h.c.l.abbenhuis@tue.nl
r.a.v.santen@tue.nl

Supporting information for this article is available on the WWW under http://www.chemeurj.org/ or from the author.

We have endeavored to immobilize TiPOSS in order to design applicable heterogeneous epoxidation catalysts.[12–14] The immobilization methods include physical adsorption into the nanopores of mesoporous silica MCM-41[12,13] and chemical grafting into a three-dimensional netted polysiloxane.[14] Both cases yield active epoxidation catalysts with *tert*-butyl hydrogen peroxide (TBHP) as the oxidant. However, when aqueous hydrogen peroxide (H_2O_2), which is more environmentally benign and cheaper than organic oxidants, was employed as the oxidant neither the homogeneous TiPOSS nor the TiPOSS supported on MCM-41 was active. This is believed to result from the irreversible hydrolysis of the siloxy–Ti bonds of TiPOSS in aqueous H_2O_2 solution.[11,14] In contrast, TiPOSS grafted into polysiloxane showed high activity under the same conditions.[14] It has been established that the hydrophobic polymer network around the TiPOSS compound can stabilize the active sites and together with the TiPOSS builds up a catalytic ensemble that resembles titanium silicate-1 (TS-1), which is currently one of the best catalysts for epoxidation of small alkenes with aqueous H_2O_2 as the oxidant.

The methods mentioned above (immobilization on inorganic solids and in organic polymers) are the two most commonly used heterogenization procedures. They each have some advantages over the other, and provide different opportunities for heterogenized catalysts that can meet special demands in different catalytic systems.[15] Inorganic supports often possess rigid porous structures and high specific surface areas and are easy to separate, while organic polymers often make the catalyst behave more homogeneously because of the better compatibility with organic reaction media. Considering this fact and our previous results for the immobilization of TiPOSS compounds, we proposed combining these two methods to synthesize porous inorganic solid-supported polymeric POSS film. The resulting catalyst should have the merits of the both methods: facilitated diffusion of reactant molecules, better accessibility of the active sites due to the rigid porous structure of the inorganic support, and improved compatibility between host and guest species and organic solvents arising from the specific properties of the organic polymer films.

There may be two complications for this synthesis strategy. First, it is necessary to avoid pore blockage by the polymer since an open porous structure is important for the accessibility of the active sites, so appropriate choices of inorganic support and the polymerization method should be made. The second challenge is to increase the stability of the polymer on the inorganic support. Ordered mesoporous silica provides an ideal support as the ordered open mesopore systems with uniform pore diameters are beneficial for diffusion and dispersion of guest species and hence will reduce the possibility of pore blockage. There have been several previous investigations of the synthesis of organic polymers inside mesoporous silica. The resulting hybrid composites showed some interesting physical properties due to the confinement of the nanopores.[16–20] However, in most cases, the entire pore volume of the mesoporous silica was filled by the incorporated polymer.[16–20] Therefore, for retaining a porous structure after the polymer incorporation, an efficient immobilization method needs to be developed. Ryoo et al.[21] reported recently that functional polymer-silica composites with well-defined mesoporosity could be obtained by in-situ polymerization of monomers adsorbed on the pore walls of mesoporous silica SBA-15. A key step to avoid pore blockage was to form a uniform monomer film on the pore wall surface of SBA-15 before polymerization by selectively removing the solvent used for the impregnation of monomers. SBA-15[22] is probably one of the best supports for the synthesis of porous organic polymer–silica composites. In addition to the ordered two-dimensional hexagonal mesoporous structure similar to MCM-41, SBA-15 presents the advantage of larger pore diameters (> 7 nm) than the MCM-41 used previously for the immobilization of POSS.[12,13] This is important for efficient diffusion and dispersion of POSS-containing monomers inside the nanopores and for reducing the risk of pore blockage. (The TiPOSS compound has a minimal diameter around 1.5 nm, roughly half of the pore diameter of MCM-41.[13]) Moreover, for most SBA-15 materials, there are complementary mesopores/micropores inside the mesopore walls connecting the mesopores in a three-dimensional porous structure,[23–26] which can help the polymer film interconnect into a three-dimensional network, interpenetrate with the silica framework, and thus increase the stability of the polymer on the silica support.[21] Quite recently, Ryoo et al. reported the synthesis of ferrocene-functionalized mesoporous polymer–silica nanocomposite materials that exhibited high activity and selectivity toward catalytic hydroxylation of phenol, which was attributed to the hydrophobic nature of the polymer surface.[27]

In the present study, we demonstrate the successful combination of two commonly used immobilization methods by integrating TiPOSS into an SBA-15-supported polystyrene film by the in-situ copolymerization method. The resulting hybrid materials have highly ordered mesoporous structures and prove to be very active heterogeneous catalysts for alkene epoxidation with TBHP or aqueous H_2O_2. Fusion of the silica support (highly porous structure, hydrophilic surface) and of the polystyrene and POSS (hydrophobic network) into one entity makes the hybrid materials behave as interfacial catalysts in epoxidation with aqueous H_2O_2 and leads to much higher activity than their homogeneous counterpart due to the hydrophobic environments around the active centers.

Results and Discussion

Synthesis and structural characterization of the vinyl-substituted POSS compound Vi-TiPOSS (2): To synthesize silsesquioxane trisilanol groups for incorporation of titanium and with vinyl groups suitable for polymerization, we adapted a base-catalyzed hydrolysis–condensation of isobutyltrimethoxysilane (iBuSi(OMe)$_3$) for the synthesis of T_7-trisilanol

POSS ($(i\text{Bu})_7\text{Si}_7\text{O}_9(\text{OH})_3$). By substituting a proportion of the iBuSi$(\text{OMe})_3$ by vinyltrimethoxysilane (ViSi$(\text{OMe})_3$) in the synthesis mixture, a series of POSS trisilanols, ViPOSS (**1**), with identical cage structures but different degrees of vinyl substitution were obtained (Scheme 1). (With only

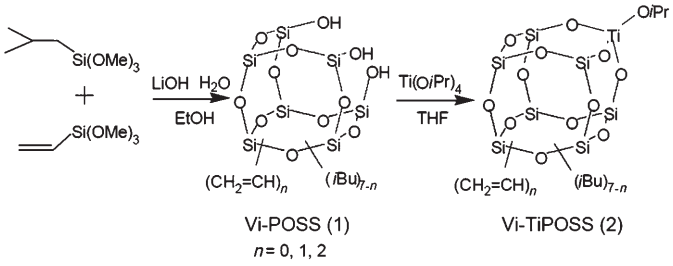

Scheme 1. Synthesis of the titanium–POSS compound Vi-TiPOSS (**2**).

ViSi$(\text{OMe})_3$ as the precursor, no trisilanol silsesquioxane was obtained.) The mixtures were analyzed by MALDI-TOF-MS (matrix-assisted laser desorption/ionization-time of flight mass spectrometry) and NMR spectroscopy. The best results were obtained with a composition of 80 mol % iBuSi$(\text{OMe})_3$/20 mol % ViSi$(\text{OMe})_3$. MALDI-TOF-MS results (Figure 1) showed that the main products consisted of T_7-tri-

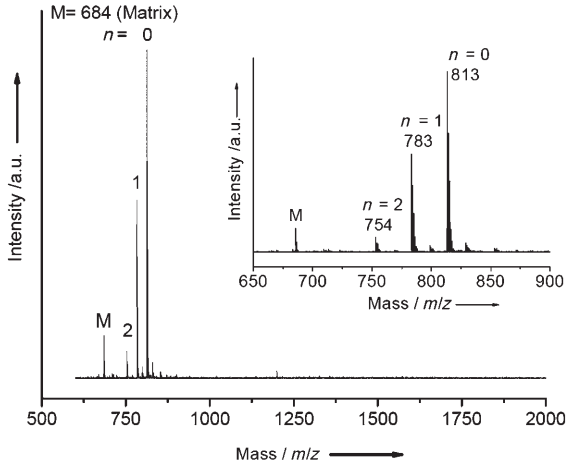

Figure 1. MALDI-TOF-MS analysis of the POSS ligand Vi-POSS (**1**). Inset: enlargement of the MALDI-TOF-MS plot.

silanol POSS with different numbers of vinyl substituents (0, 1, and 2) and negligible impurities. ^{1}H NMR and ^{13}C NMR results confirmed the presence of silanol groups in the POSS compounds with signals around $\delta = 6.60$ ppm as well as the vinyl group around $\delta = 5.95$ ppm. To incorporate the titanium center into the POSS, reaction of trisilanol mixture **1** with Ti$(\text{O}i\text{Pr})_4$ afforded the titanium-containing Vi-TiPOSS (**2**). ^{1}H NMR spectroscopy showed that with the virtual complete disappearance of silanol groups, new signals corresponding to an isopropyl group were obtained, indicating that **2** had been synthesized successfully.

Synthesis of the PS-TiPOSS/SBA-15 hybrid materials: We chose SBA-15 silica as the support material. It was synthesized with controlled microporosity by the procedure reported by Ryoo et al.[25] The XRD pattern proved the highly ordered *P6mm* mesostructure (Figure 2). Nitrogen sorption

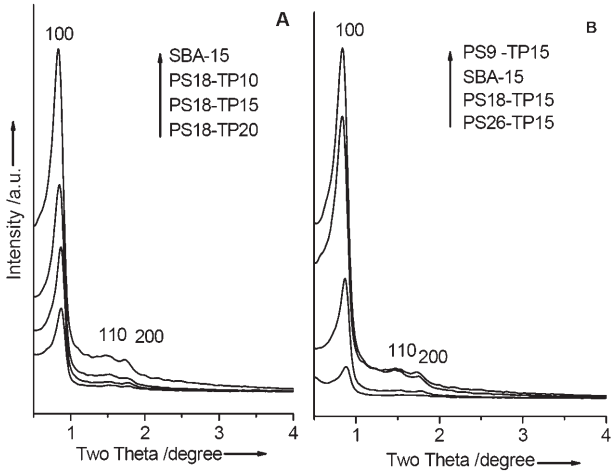

Figure 2. XRD patterns of SBA-15 and the hybrid catalysts: A) PS18-TPy; B) PSx-TP15.

data showed the typical textural properties of SBA-15: large BET surface area ($S_{\text{BET}} \approx 880\ \text{m}^2\text{g}^{-1}$) and total pore volume ($V_t \approx 1.05\ \text{cm}^3\text{g}^{-1}$), uniform pore size distribution ($D_{\text{BJH}} \approx 7.6$ nm), and considerable micropore surface area ($S_{\text{mic}} \approx 309\ \text{m}^2\text{g}^{-1}$) and micropore volume ($V_{\text{mic}} \approx 0.14\ \text{cm}^3\text{g}^{-1}$) (Table 1). As mentioned above, S_{mic} and V_{mic} are important for interconnection of the polymer film into a three-dimensional network.

The synthetic procedure for PS-TiPOSS/SBA-15 hybrid materials is shown in Scheme 2. It is difficult to build up a polymer with **2** as the sole precursor because of the structure of compound **2** and resulting steric hindrance. We therefore added styrene and divinylbenzene (DVB, crosslinker) to copolymerize **2** into the polymer backbone. The known polymerization chemistry and high stability of polystyrene make it an ideal choice. Moreover, polystyrene can provide a hydrophobic environment for TiPOSS that is beneficial to the performance of the resulting hybrid catalysts.[14,27]

To avoid blockage of the porous structure by the PS-TiPOSS copolymer, it is vital to achieve a uniform distribution of the monomers inside the mesopores of SBA-15 before the polymerization reaction. We used the evaporation-induced adsorption method,[21,26] which is believed to help the formation of a uniform monomer film and enhance the interaction between the monomers and the silica support. After impregnation of the monomers the solvent dichloromethane was selectively removed, then styrene/DVB

Table 1. Textural parameters of PS-TiPOSS/SBA-15 samples with different compositions.

Sample	d_{100}[a] [nm]	D_{BJH}[b] [nm]	S_{BET}[c] [m^2g^{-1}]	S_{mic}[d] [m^2g^{-1}]	S_p[d] [m^2g^{-1}]	S_{ext}[d] [m^2g^{-1}]	V_t[e] [cm^3g^{-1}]	V_{mic}[f] [cm^3g^{-1}]	V_p[f] [cm^3g^{-1}]	Ti[g] [wt%]
SBA-15	10.6	7.6	888	309	545	34	1.05	0.14	0.85	–
PS9-TP15	10.5	6.6	580	164	388	28	0.71	0.070	0.59	0.52
PS18-TP15	10.2	6.5	534	133	377	24	0.65	0.055	0.55	0.58
PS26-TP15	10.0	6.5	477	112	341	24	0.59	0.045	0.50	0.58
PS36-TP15	10.2	6.2	383	82	282	19	0.46	0.031	0.40	0.56
PS18-TP10	10.4	6.8	540	106	407	27	0.72	0.054	0.62	0.42
PS18-TP20	10.1	6.5	510	132	354	24	0.62	0.055	0.52	0.77

[a] d_{100} values obtained from XRD patterns. [b] Pore diameter determined from the adsorption branches of nitrogen sorption isotherms by the BJH method. [c] S_{BET} is the BET surface area. [d] S_{mic}, S_{ext}, and S_p are the micropore surface area, external surface area, and primary mesopore surface area, respectively, all calculated from the t plots. [e] V_t is the total pore volume determined at the relative pressure of 0.98. [f] V_{mic} and V_p are the micropore volume and the primary mesopore volume respectively, calculated from the t plots. [g] Titanium contents were determined by ICP analysis.

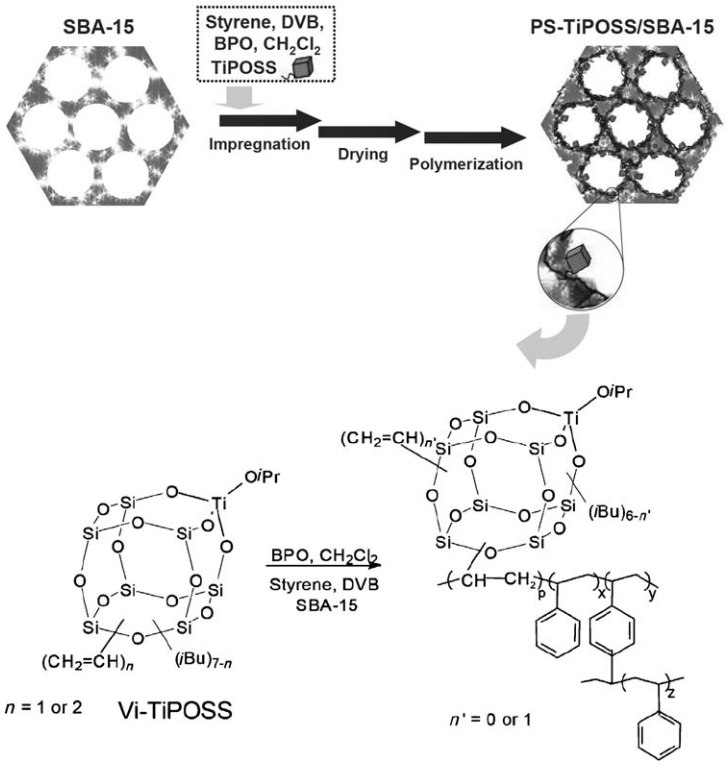

Scheme 2. Schematic presentation of the procedure for synthesis of PS-TiPOSS/SBA-15 hybrid materials.

and **2** were copolymerized in the solid state and washed with chloroform to remove the unincorporated monomers. The structure of the resulting hybrid materials was characterized by a series of techniques. Samples thus obtained were denoted as PSx-TPy, in which PS = polystyrene, TP = Vi-TiPOSS (**2**), and x and y are their respective percentages by weight relative to the silica to the silica-supported catalyst.

Textural properties of the PS-TiPOSS/SBA-15 hybrid materials: Figure 2 displays the XRD patterns of the samples with different PS/POSS compositions. A sharp diffraction peak (100) is observed for all the hybrid materials. This indicates that the ordered *P6mm* mesoporous structure was retained after coating with the PS-TiPOSS polymer. For most samples, an increase in the contents of PS and POSS resulted in lowered intensity of the (100) peak, which is often the case for surface-modified mesoporous materials.[28] This implies that the PS-POSS polymer is located inside the mesopores, which usually lowers the scattering contrast of X-ray between the pore space and the pore wall, and hence decreases the intensity of the (100) peak.[29] Exceptionally, sample PS9-TP15 showed higher (100) peak intensity than SBA-15. This is contrary to the decrease in intensity usually observed for most surface-modified mesoporous materials, but is consistent with the results previously reported.[21,26] Because of the roughness of the inner surface of SBA-15 caused by the presence of micropores in the pore walls,[23–25] during the evaporation of the solvent, monomers at a low loading will preferentially occupy the micropores due to capillarity and the concavities of the pore wall surface, driven by the surface tension. This will result in a smoother surface and enhanced contrast of X-ray scattering between the pore space and the pore wall.

Textural properties of the hybrid materials were characterized by nitrogen sorption measurements. All samples show type IV isotherms with steep H1 hysteresis loops at relative pressure P/P_0 around 0.6–0.8 (Figure 3), which is characteristic of materials with uniform mesopore diameter. This indicates absence of pore blockage for all the samples. After coating with the polymer, the onset values of monolayer–multilayer adsorption on the isotherms decreased remarkably, suggesting that a considerable proportion of the micropores were filled with the polymer. With the increase of POSS and polystyrene loadings, the BET surface area S_{BET}, total pore volume V_t, and Barrett–Joyner–Halenda (BJH)[30] pore diameters D_{BJH} decreased gradually, which

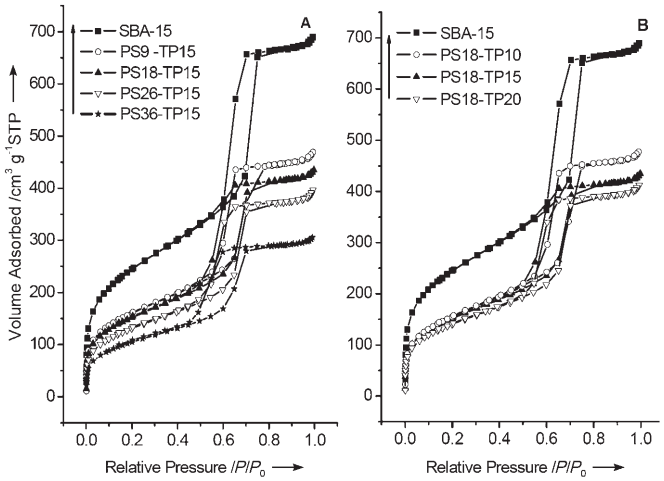

Figure 3. Nitrogen sorption isotherms of SBA-15 and the hybrid catalysts A) PS*x*-TP15 and B) PS18-TP*y*.

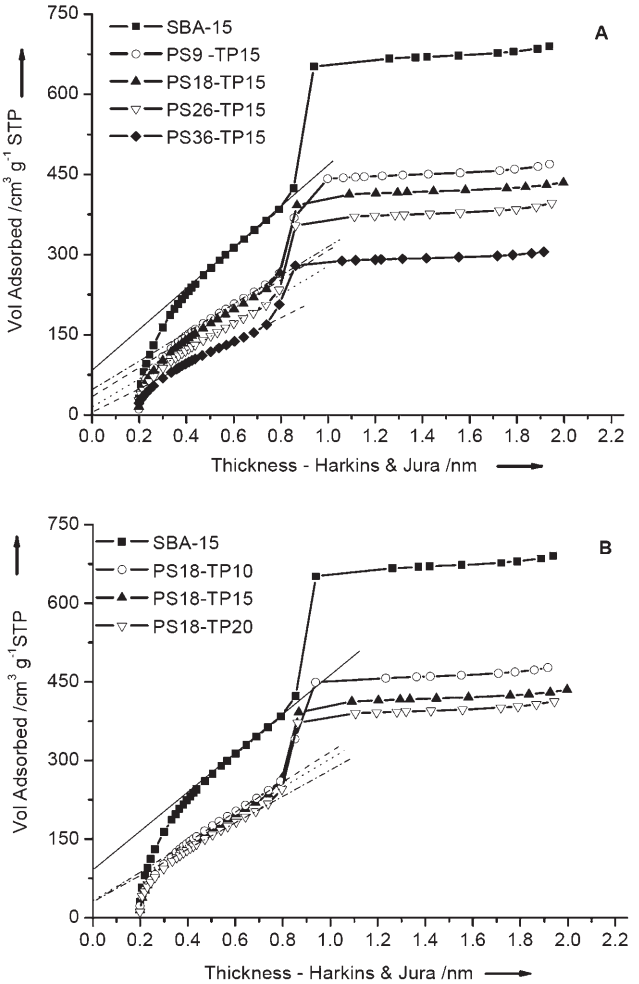

Figure 4. *t* plots of SBA-15 and the hybrid catalysts A) PS*x*-TP15 and B) PS18-TP*y*.

further confirms that coating of the polymer film occurred on inner surfaces of the mesoporous silica (Table 1). No tailing of the desorption branches to the lower limit (at a relative pressure of ≈0.40–0.50) of nitrogen adsorption–desorption hysteresis at 77 K[31] was observed for any sample, which means that the mesopores were open without being plugged by the polymer.[32] For all the samples, highly centered pore size distributions were observed (Figures S1 and S2: the BJH pore size distributions derived from the adsorption branches of the isotherms), which indicates that the PS-POSS copolymer was distributed homogeneously inside the mesopores. With an increase in polymer loading, the pore size decreases gradually. This provides an opportunity for tuning the pore size of mesoporous materials and the surface properties at the same time.

To evaluate the location and distribution of the polymer further, comparative *t* plots of samples with different compositions were calculated.[33] In Figure 4A, the *y* axis intercept values of the extrapolated lines from the first linear parts of the *t* plots decrease gradually with an increase in the polystyrene content, which results from a decrease in the micropore volume V_{mic} and indicates the filling of the micropores by polystyrene (see also Table 1). As mentioned previously, this will help the polymer to interconnect to form an interpenetrating structure with the silica wall, resulting in a physically inseparable hybrid composite. In contrast, for samples with different POSS contents and the same PS content, the micropore volume remains almost constant (Figure 4B and Table 1). This can be explained by the fact that the diameter of TiPOSS compound is about 1.5 nm and thus it can not enter the micropores easily, especially given the competitive adsorption by the relatively small styrene molecules. With an increase in the TiPOSS content, the *y* axis intercept values of the second linear portions of the *t* plots, corresponding to the sum of primary mesopore volume V_p and micropore volume V_{mic}, decrease gradually. Thus, the TiPOSS compounds should mostly be located inside the mesopores and coat the pore wall surfaces instead of being embedded in the pore walls, which is beneficial for high accessibility of the active sites to the reactants. From Table 1, it is clear that the primary mesopore volume V_p and mesopore surface area S_p decrease when TiPOSS and polystyrene contents increase, while only small changes were observed in the external surface area S_{ext}. This implies that the polymer coating was mainly on the inner surface of the SBA-15. To confirm this conclusion, SEM and TEM (scanning and transmission electron microscopy, respectively) measurements of the samples were made.

Figure 5 shows that the highly ordered *P6mm* mesostructure of sample PS18-TP15 was preserved after the polymer coating was applied, as evidenced by the images of mesopores arrayed in hexagonal symmetry ([100] direction) and straight mesopores arrayed in a parallel fashion ([110] direction). No bulk polymer phase outside the SBA-15 particle has been detected, as further confirmed by the SEM images of pristine SBA-15 and sample PS26-TP15 in Figure 6. After coating with the polymer, the short, curved,

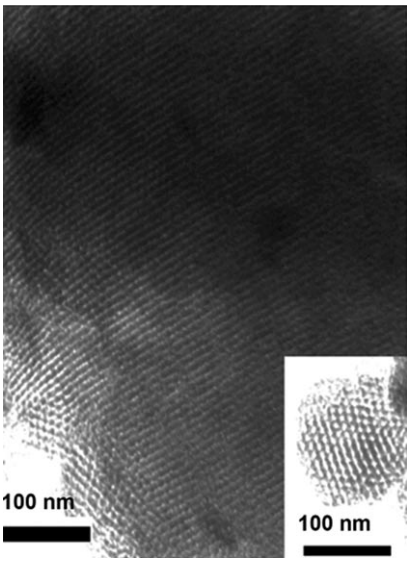

Figure 5. TEM images of the hybrid catalyst PS18-TP15.

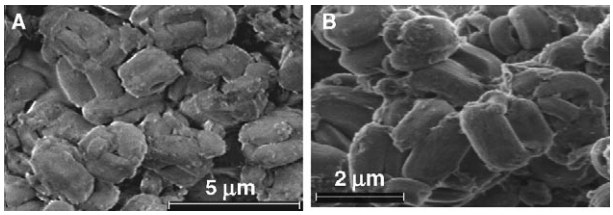

Figure 6. SEM images of A) SBA-15 and B) the hybrid catalyst PS26-TP15.

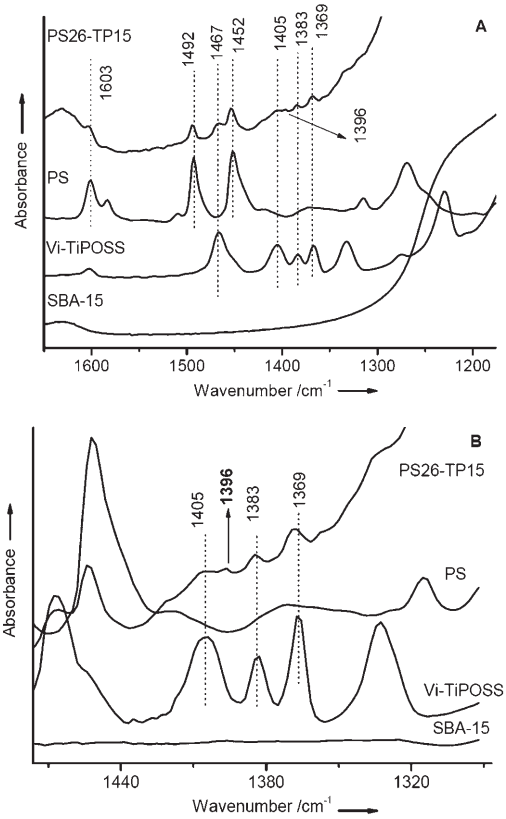

Figure 7. A) IR spectra of SBA-15, Vi-TiPOSS (**2**), polystyrene (PS), and sample PS26-TP15. B) Enlargement of the spectra in A.

rod-like morphology of SBA-15 was retained; no bulk polymer phase was observed.

All the characterizations have confirmed that the PS-TiPOSS polymer was coated on the inner surface of the SBA-15. The resulting hybrid PS-TiPOSS/SBA-15 materials possessed a highly ordered mesostructure with an open pore system, and a large specific surface area ($>380\ m^2 g^{-1}$) and pore volume ($\geqq 0.46\ cm^3 g^{-1}$).

Chemical compositions of the PS-TiPOSS/SBA-15 hybrid materials: Comparison of the IR spectra of SBA-15, polystyrene, Vi-TiPOSS, and sample PS26-TP15 (Figure 7) showed the presence of both components in the hybrid materials polystyrene (C=C stretching vibration band at 1603 cm^{-1} and alkyl chain C–H vibration bands at 1492 and 1452 cm^{-1})[34] and Vi-TiPOSS (C–H vibration bands at 1467, 1405, 1383, and 1369 cm^{-1}). Compared with Vi-TiPOSS and polystyrene, a new peak around 1396 cm^{-1} was observed for sample PS26-TP15 (Figure 7B). We tentatively attribute this peak to the C–H vibration of the methylene or methine group that links the POSS into the polystyrene chain.

The ^1H-^{13}C CP-MAS-NMR spectrum of sample PS26-TP15 (Figure 8A) shows peaks from polystyrene ($\delta =$ 41 ppm for backbone methylene and methine carbons, 129 ppm for protonated aromatic carbon, 138 ppm for the remnant vinyl carbon, and 148 ppm for the quaternary aromatic carbon)[35] as well as peaks from the isobutyl groups of the POSS unit ($\delta = 24$ ppm), confirming the successful immobilization of both components. To find further proof of the copolymerization of styrene with Vi-TiPOSS, we synthesized two polymers with the same PS/TiPOSS weight ratio with sample PS26-TP15 but without the SBA-15 support. Sample PS26-TP15-poly was a polymer synthesized in toluene without an SBA-15 support. Sample PS26-*i*Bu-TP15-poly was a polymer synthesized by the same method as PS26-TP15-poly but from a non-vinyl-substituted POSS, (i-$C_4H_9)_7Si_7O_{12}Ti(Oi\text{-}C_3H_7)$ (**3**). It was therefore a physical mixture of polystyrene and TiPOSS. A comparison of the ^1H-^{13}C CP-MAS-NMR spectra of these samples showed that a new peak around $\delta = 18$ ppm arose for PS26-TP15 and PS26-TP15-poly. Thus, it was very likely to have originated from the methylene or methine carbon atoms at the anchor point of TiPOSS into the polystyrene chain (Figure 8B). Simulation with ChemDraw 8.0 (Cambridgesoft) gave a rough estimate of the chemical shifts of the methine and the methylene carbon atoms around $\delta = 21$ and 26 ppm, respectively. Thus, the peak at $\delta = 18$ ppm can be ascribed to the anchor point methine carbon atom as proof of the copolymerization between styrene and Vi-TiPOSS and further evidence for chemical bonding between POSS and PS polymer chains.

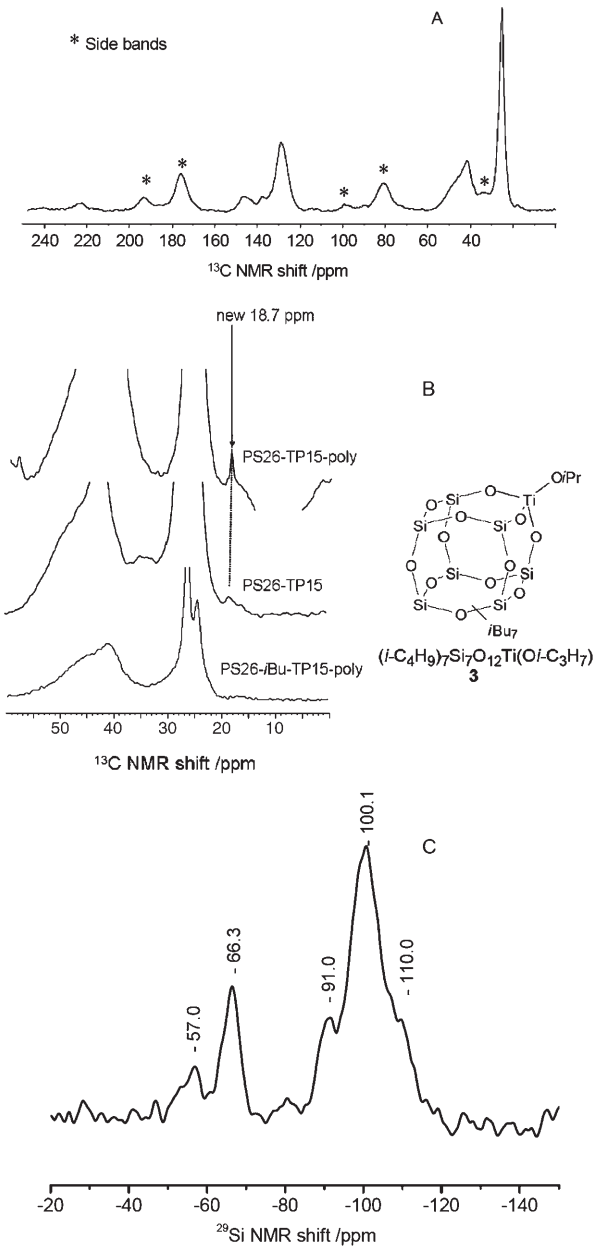

Figure 8. A) ^{1}H-^{13}C CP-MAS-NMR of the hybrid catalyst PS18-TP15. B) Comparative ^{1}H-^{13}C CP-MAS-NMR data of the hybrid catalyst PS26-TP15, PS26-TP15-poly (copolymer of polystyrene and Vi-TiPOSS in weight ratio 26:15), and PS26-*i*Bu-TP15-poly (polymer of polystyrene and **3** synthesized with weight ratio 26:15). C) ^{1}H-^{29}Si CP-MAS-NMR spectrum of the hybrid catalyst PS26-TP15.

The ^{1}H-^{29}Si CP-MAS-NMR spectrum of sample PS26-TP15 shows the presence of both the Q^n sites ($(SiO)_nSi(OH)_{4-n}$, $Q^2 \approx -91$, $Q^3 \approx -100$, and $Q^4 \approx -110$) from the silica support and T^n sites ($(SiO)_nSiR(OH)_{3-n}$) from the TiPOSS units (Figure 8C). Peaks at $\delta = -57$ and -66 ppm were ascribed to T^2- and T^3-site Si atoms attached to isobutyl groups, respectively.

To evaluate the actual loading of the polymer, thermal gravimetric analysis (TGA) was performed under an air flow from room temperature to 900 °C. TGA results show that more than 80 wt % of the initial mixture was incorporated into the hybrid materials. It is interesting that for PS*x*-TP15 samples when polystyrene content was increased, the decrease in weight loss below 150 °C corresponding to adsorbed water and other volatiles was not proportional to the decrease in their pore volumes (see Figure 9 and Table 1).

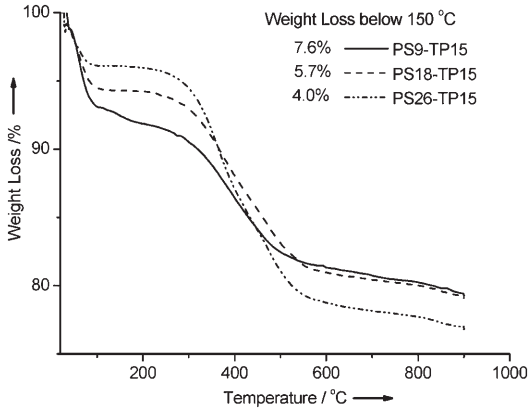

Figure 9. TGA results of the hybrid catalysts PS*x*-TP15.

This should be attributed to the enhanced hydrophobicity of the hybrid materials with an increase in the polystyrene loadings. Titanium contents (listed in Table 1) were determined with ICP (inductively coupled plasma) measurements. The loadings of titanium lay in the range 0.42–0.77 wt %. All of the above results confirm that PS-TiPOSS copolymer has been immobilized successfully on SBA-15.

UV Raman spectroscopy is a powerful technique for the selective identification of site-isolated transition metal centers in zeolites and mesoporous materials.[36] Raman spectra with an excitation line in the ultraviolet region give better signal-to-noise ratios than when excitation occurs in the visible region, mainly because UV Raman spectroscopy can avoid most of the fluorescence interference that often gives bands in the 300–700 nm region.[36] Moreover, another advantage of UV Raman spectroscopy over visible Raman spectroscopy is due to the "resonance Raman effect."[36] Since the absorption bands of the charge-transfer transition between the oxygen anion and the framework transition-metal cation often lie in the ultraviolet region, excitation by laser light with a wavelength in the ultraviolet range can selectively enhance the Raman bands directly associated with the isolated framework metal center for metal-containing zeolites and mesoporous materials.[37] Specifically, the isolated framework titanium species has been identified unambiguously by UV Raman spectroscopy.[37–39] Considering the structural similarity between Vi-TiPOSS (**2**) and TS-1 zeolite, UV Raman spectra are expected to provide important information about the status of the titanium species in the PS-TiPOSS/SBA-15 hybrid materials.

Figure 10A displays the UV Raman spectra of trisilanol POSS Vi-POSS (**1**), titanium-containing POSS Vi-TiPOSS

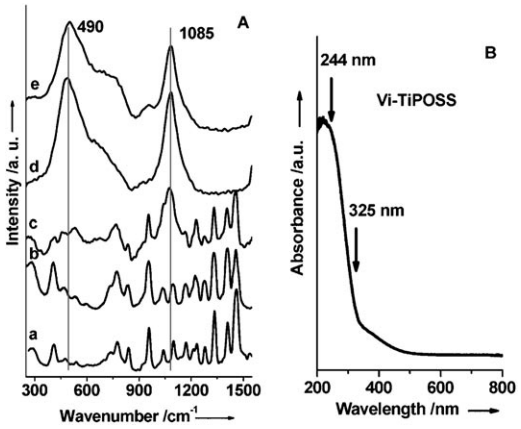

Figure 10. A) UV Raman spectra of compounds Vi-POSS (**1**), Vi-TiPOSS (**2**), and PS18-TP15, with excitation laser lines at 325 nm and 244 nm. a) Vi-POSS ($\lambda_{ex}=325$ nm); b) Vi-POSS ($\lambda_{ex}=244$ nm); c) Vi-TiPOSS ($\lambda_{ex}=325$ nm); d) Vi-TiPOSS ($\lambda_{ex}=244$ nm); e) PS18-TP15 ($\lambda_{ex}=244$ nm). B) UV/Vis diffuse reflectance spectrum of Vi-TiPOSS.

(**2**), and the hybrid material PS18-TP15 with excitation laser lines at 325 nm and 244 nm. For **1**, different excitation lines gave identical Raman bands associated with the cage structure of trisilanol POSS units (spectra a and b). After the incorporation of titanium, **2** (spectrum c, excitation laser line at 325 nm) gave a new peak around 1085 cm^{-1}. When the 244 nm excitation line was utilized for the same sample, this peak became more prominent, while another strong peak appeared at 490 cm^{-1} (spectrum d). Based on the previous UV Raman investigations on TS-1 and other titanium-containing materials,[37–39] we attribute the bands at 490 and 1085 cm^{-1} to the bending and asymmetric vibrations of Si-O-Ti species associated with a tetrahedrally coordinated titanium center. In contrast to **1**, compound **2** gave distinct Raman spectra when different excitation lines were used. This phenomenon originates from the resonance Raman effect, as mentioned above. Figure 10B shows the UV/Vis diffuse reflectance spectrum of **2**. The 244 nm line is in the absorbance band of the electronic absorption of **2**, which originates from the charge-transfer transition between the titanium and ligand oxygen atoms in the isolated TiO_4 units of **2**, as is often observed in the titanium-containing zeolites.[37] Thus, excitation with the 244 nm line can selectively enhance the Raman bands associated with the isolated titanium species. It is interesting that the frequency of the band at 1085 cm^{-1} is lower than those for TS-1 (1125 cm^{-1})[37] and Ti-MCM-41 (1100 cm^{-1}),[38a] and similar to that of the highly dispersed titanium species on silica (Ti/SiO_2).[39] This difference in frequency essentially reflects the difference in the coordination environments of the titanium centers. For sample PS18-TP15, no indicative information can be obtained with an excitation line at 325 nm due to the strong fluorescence interference (data not shown). In contrast, when a 244 nm laser line was used, a spectrum similar to that of **2** was obtained (spectrum e, Figure 10A). These results elucidate the site-isolated nature of the titanium in the hybrid materials and show that no evident changes occurred around the titanium center during the immobilization process.

Epoxidation of cyclooctene with PS-TiPOSS/SBA-15 hybrid materials with TBHP as the oxidant: To test the effectiveness of the present immobilization method, epoxidation reactions of cyclooctene with TBHP or aqueous H_2O_2 as the oxidant were performed for the hybrid materials.

All the catalysts showed high activity in the epoxidation of cyclooctene, with selectivities over 90% and comparable TOFs to the homogeneous counterparts when TBHP was used as the oxidant (Table 2). Figure 11 displays results for the different hybrid catalysts as well as the homogeneous counterpart Vi-TiPOSS (**2**). The homogeneous catalyst shows a second-order kinetic behavior, which is consistent with our previous results.[11,12] Second-order kinetic behavior is also observed for all the hybrid catalysts. Moreover, the rate constants of the hybrid catalysts are of the same order and comparable with that of homogeneous catalyst **2**. This suggests that the active sites of the catalyst are highly accessible and the reactants can diffuse efficiently into the nanopores of the hybrid catalysts, which should be attributed to the open pore system and the hydrophobic surface properties. The highest rate constant was obtained with sample PS18-TP15. This indicates that there should be an optimal composition of TiPOSS and polystyrene, resulting in a balance between the active-site loadings, the hydrophobicity, and the structural properties.

Table 2. Epoxidation results for PS-TiPOSS/SBA-15 samples with TBHP as the oxidant.[a]

Sample	Conv.[b] [%]	Yield[b] [%]	TOF[c] [mmol $mmol^{-1}$ h^{-1}]
Vi-TiPOSS[d]	99	99	319
PS9-TP15	94	92	207
PS18-TP15	98	97	235
PS26-TP15	94	88	220
PS18-TP10	94	88	241
PS18-TP20	95	90	169
PS26-TP15 (r1)[e]	87	84	–
PS26-TP15 (r2)[e]	93	91	–
PS26-TP15 (r3)[e]	86	83	–
PS26-TP15 (r4)[e]	91	87	–
PS26-TP15 (r5)[e]	70	67	–
PS26-TP15 (r6)[e]	75	74	–
PS26-TP15 (r7)[e]	83	77	–

[a] All reactions were performed at 60 °C in isooctane with [TBHP] = [cyclooctene] = 1.29 M, [Ti] = 0.005 M, and 1,3,5-trimethylbenzene as GC internal standard. [b] Conversion and yield were determined by GC after 17 h. [c] Initial turnover frequency (TOF) determined after 0.5 h. [d] Homogeneous catalyst Vi-TiPOSS. [e] Recycling tests with catalyst PS26-TP15 (r*x*), wherein r denotes "recycle" and *x* is the recycle sequence.

We also tested the recyclability of the hybrid catalysts. The catalyst can be recycled at least seven times without a significant decrease in conversion and yield (Table 2). This result proves that the hybrid catalysts synthesized with this novel immobilization method are robust and can be recycled.

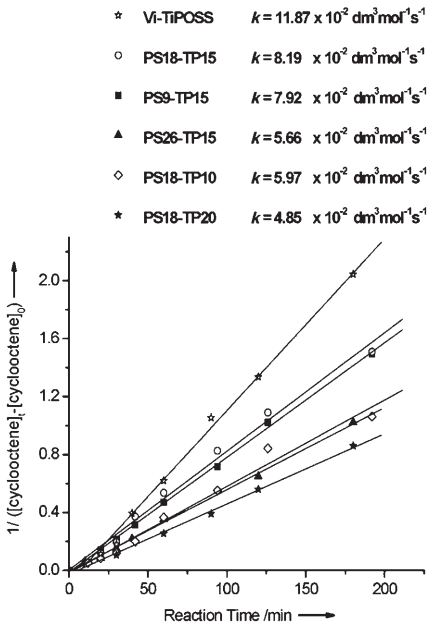

Figure 11. Kinetic investigations of cyclooctene epoxidation with Vi-TiPOSS (**2**) and the hybrid catalysts PS*x*-TP*y*. [TBHP] = [cyclooctene] = 1 M, [Ti] = 0.001 M. The reaction was performed at 60 °C. At suitable time intervals, samples (each 0.1 mL) were taken from the reactors, filtered through syringe filters (0.45 μm), injected into GC vials containing MeOH (0.9 mL), and analyzed by GC.

Epoxidation of cyclooctene with PS-TiPOSS/SBA-15 hybrid materials with aqueous H_2O_2 as the oxidant: Compared with TBHP, aqueous H_2O_2 has several advantages such as low cost and environmentally benign character, generating water as the only co-product. We tested the capability of the hybrid PS-TiPOSS/SBA-15 catalysts in epoxidation with aqueous H_2O_2 as the oxidant.

Figure 12 compares the catalytic performances of the hybrid catalyst and the homogeneous TiPOSS compound **3** in the epoxidation of cyclooctene. Much higher yields (> 25 %, based on the H_2O_2 used) and TOF (> 79, determined at a reaction time of 30 min) could be obtained with the heterogeneous hybrid catalyst than with the homogenenous counterpart (yield 8.4 %, TOF 33). The highest yield (70 %) was obtained with the catalyst PS26-TP15. This is comparable with the results obtained from the polysiloxane-grafted TiPOSS.[14] In aqueous H_2O_2, the TiPOSS compound may suffer irreversible hydrolysis of its siloxy–titanium bonds.[11] This accounts for the inactivity of homogeneous TiPOSS and the physically adsorbed TiPOSS in MCM-41 for epoxidation with aqueous H_2O_2. In contrast, TiPOSS grafted into three-dimensional siloxane polymer showed high activity.[14] It is believed that the polymer around TiPOSS can protect the titanium sites against hydrolysis by water. The resulting catalytic ensembles resemble TS-1. They combine a multipodal titanium site with a strongly hydrophobic environment.[14] The high activity for the present hybrid catalysts is derived from the hydrophobic polystyrene surroundings around the TiPOSS. As a further proof, increasing the PS content, that is, the enhancement of the hydrophobic environment, leads to a higher yield and TOF (Figure 12).

In addition to the shielding effect, the hydrophobic surface properties in our catalyst can also provide better compatibility with the reactants than the TiPOSS adsorbed onto MCM-41 silica. Diffusion of the reactants and the products may be more efficient. As a consequence of the hydrophobicity, our hybrid catalysts behave as interfacial catalysts in the two-phase reaction media. Different surface properties result in totally different phase locations of mesoporous silica SBA-15 and the hybrid PS-TiPOSS/SBA-15 catalyst. In the reaction media, SBA-15 silica is separated in the lower aqueous layer, while the hybrid catalyst remains at the interface between the oil phase of cyclooctene and the aqueous phase of H_2O_2 (Figure 13). This phenomenon should result from the synergetic effect of the hydrophobicity of polystyrene and POSS, the hydrophilicity of silica, and the low framework density caused by the mesoporous structure. It provides increased interactions between the reactant,

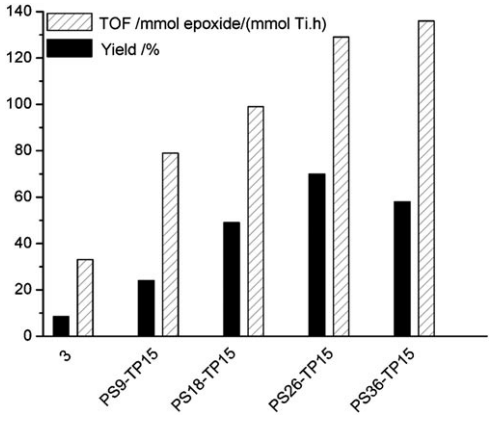

Figure 12. Epoxidation results of cyclooctene with POSS compound **3** (*i*-$C_4H_9)_7Si_7O_{12}Ti(Oi\text{-}C_3H_7)$ and the hybrid catalysts PS*x*-TP15 in aqueous H_2O_2 (35 wt %). All the reactions were performed at 60 °C for 17 h with molar ratios cyclooctene/H_2O_2 = 4:1, H_2O_2/Ti = 250:1, and TMB as the GC internal standard. The yields were based on amount of oxidant used. TOF was calculated by the yield at 0.5 h after the reaction started.

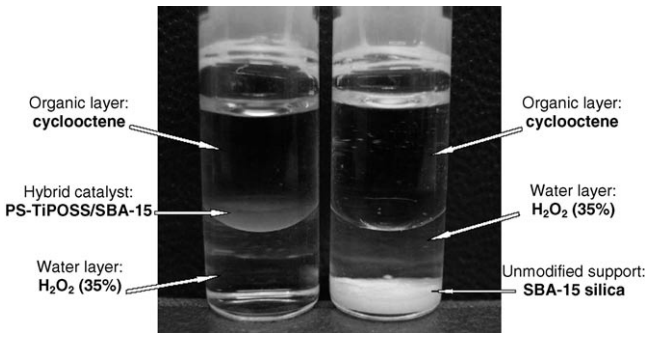

Figure 13. Comparison of the locations of SBA-15 and the hybrid catalyst PS18-TP15 in the reaction media composed of cyclooctene (upper layer) and aqueous H_2O_2 (lower layer, 35 wt %) after thorough homogenization of the mixtures by ultrasonic treatment for 5 min and aging for 2 h.

the oxidant, and the catalytic sites, and hence increases the probability of reaction in the two-phase reactions in comparison with catalysts that are only water-soluble or only oil-soluble.

To evaluate the effectiveness of the current immobilization method further, catalysts with the same PS/TiPOSS ratio but synthesized by different methods have been compared. The results of epoxidation with aqueous H_2O_2 are shown in Figure 14. P26-*i*Bu-TP15 is a catalyst synthesized

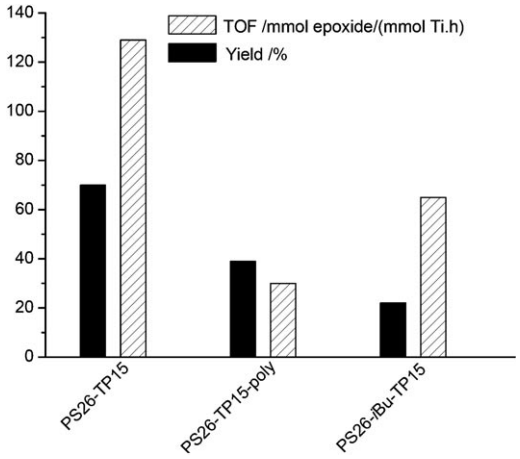

Figure 14. Comparison of the activity of different catalysts in cyclooctene epoxidation with aqueous H_2O_2. (PS26-TP15-poly: copolymer of polystyrene and **2**, weight ratio 26:15; PS26-*i*Bu-TP15: hybrid catalyst synthesized with polystyrene (26 wt%) and **3** (15 wt% relative to the SBA-15 support). All the reactions were performed at 60°C for 17 h with molar ratios cyclooctene/H_2O_2 = 4:1, H_2O_2/Ti = 250:1, and TMB as the GC internal standard. The yields were based on amount of oxidant used. TOF was calculated as the yield at 0.5 h after the reaction started.

from **3** by the same procedure as PS26-TP15. Without the vinyl substitution, the POSS **3** can thus be only physically trapped in the hybrid materials. The best result was obtained with sample PS26-TP15. Comparison between PS26-TP15 and PS26-*i*Bu-TP15 clarifies the importance of the covalent linkage between TiPOSS and polystyrene, which increases the TiPOSS–polystyrene and TiPOSS–silica interactions, and hence enhances the stability of TiPOSS. Comparison of PS26-TP15 with PS26-TP15-poly shows that the rigid porous structure is important to achieve high activity due to the fast diffusion and high accessibility of active sites induced by the open pore system. This rigid porous structure of SBA-15, the hydrophobic environment around the titanium center, and the covalent anchoring of TiPOSS to the hydrophobic polymer chain are all indispensable contributions for the excellent performance of TiPOSS in epoxidation using aqueous H_2O_2 as the oxidant.

We also tested the recyclability of the hybrid catalyst in cyclooctene epoxidation with aqueous H_2O_2. Figure 15 shows the results of recycling the hybrid catalysts with different polystyrene loadings. After the first run, the activity of all the catalysts had decreased; elemental analysis by ICP indicated that the titanium content had not decreased much

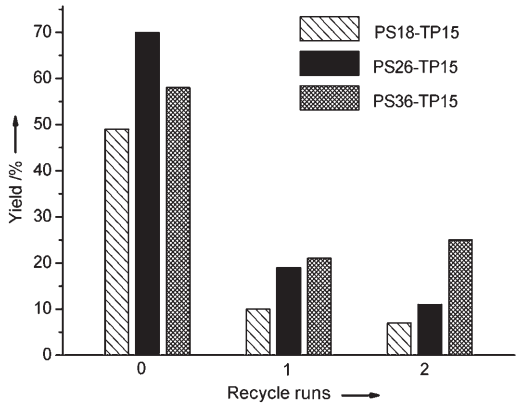

Figure 15. Recycling tests on catalysts PS*x*-TP15 in the epoxidation of cyclooctene with aqueous H_2O_2. See the Experimental Section for details.

(for PS26-TP15, 0.58 wt% versus 0.56 wt%). As mentioned above, TiPOSS units can decompose into trisilanol POSS and catalytic inactive titanium species in aqueous H_2O_2 solution.[11] The decrease in activity may be due to the gradual hydrolysis of TiPOSS into non-active titanium species, producing a decrease in the number of active sites and deposition of the inactive titanium species in a hybrid catalyst, which may induce nonproductive decomposition of H_2O_2 and thus decrease the efficiency of the H_2O_2 in the subsequent runs. The mechanism of deactivation is still under investigation.

Comparison of the recyclability of the hybrid catalysts with different polystyrene contents reveals that a higher activity in the subsequent runs can be obtained with an increase of polystyrene content. Thus, the enhancement in the hydrophobicity around TiPOSS helps to stabilize the active sites. Therefore, by optimizing the synthesis parameters (for example, by balancing the textural properties and the extent of hydrophobization, tuning the structure of TiPOSS), it may be possible to develop a highly active and robust heterogeneous catalyst using the present immobilization method for the epoxidation of large molecules with aqueous H_2O_2.

Conclusion

We have synthesized a novel mesoporous hybrid material by coating polystyrene–TiPOSS copolymer on the surface of mesoporous silica SBA-15 by means of the in-situ polymerization method. The resulting materials are highly ordered mesoporous composites and show high activity in the epoxidation of cyclooctene with TBHP or aqueous H_2O_2 as the oxidant. The present synthesis strategy combines the use of conventional immobilization methods for homogeneous catalysts; that is, it uses both inorganic solid and organic polymer support materials. The properties of the hybrid catalysts, including high accessibility of the active sites, hydrophobicity of the environment around the active sites, ease of separation, and recyclability, were improved in comparison with previously reported systems using each single immobili-

zation method. Combination of the properties of mesoporous silica supports and polystyrene-TiPOSS polymers made the hybrid catalysts behave as interfacial catalysts. We have demonstrated that a rigid porous structure, chemical bonding, predefined active sites, and hydrophobic surroundings are important factors to achieve high performance of the catalysts. We believe that this immobilization method should be applicable to a wide range of homogeneous catalysts, especially in cases in which a hydrophobic environment is demanded and/or in which a two-phase reaction is involved.

Experimental Section

Synthesis of vinyl-substituted trisilanol POSS, Vi-POSS (1): Vinyl-substituted trisilanol POSS compounds were synthesized by a LiOH-catalyzed hydrolysis–condensation method. In a typical synthesis, a suspension was obtained by adding $LiOH{\cdot}H_2O$ (3.3 g, 0.079 mol; Merck, LiOH > 56 wt%) to a solution of ethanol (75 mL) and water (1.0 mL, 0.055 mol) in a flask (0.5 L). A mixture of isobutyltrimethoxysilane (15.3 mL, 0.08 mmol; Aldrich, 97%) and vinyltrimethoxysilane (3.1 mL, 0.02 mmol; Merck, 97%) was added slowly and the reaction was left to reflux overnight, then cooled to room temperature. Pentane (100 mL) was added and the solution was stirred for 30 min. After separation of the organic layer, washing three times with an aqueous HCl solution (100 mL, 4 wt%) and evaporation of the solvent, a sticky white solid (≈10.3 g) was obtained from the organic phase. The product was analyzed by MALDI-TOF-MS and NMR spectroscopy. ^{1}H NMR of **1** (200 MHz, $CDCl_3$, 25°C): $\delta = 6.60$ (br s, 3H; OH), 5.95 (br m, 3H; $-CH{=}CH_2$ and $-CH{=}CH_2$), 1.85 (m, 6H; −CH−), 0.95 (m, 36H; $-CH_3$), 0.59 ppm (m, 12H; $-CH_2-$); MALDI-TOF MS: *m/z*: 813 $[(C_4H_9)_7Si_7O_{12}H_3]$ + Na, 783 $[(C_2H_3)(C_4H_9)_6Si_7O_{12}H_3]$ + Na, 754 $[(C_2H_3)_2(C_4H_9)_5Si_7O_{12}H_3]$ + Na.

Synthesis of titanium-containing POSS, Vi-TiPOSS (2): $Ti(OiPr)_4$ (1.57 g, 5.5 mmol; Aldrich, 97%) was added under argon to a solution of POSS trisilanol mixture **1** (3.95 g, ≈5.1 mmol) dissolved in THF (50 mL) and the reaction was left to reflux for 2 h at 50°C. Evaporation of the solvents in vacuum gave the product **2** as a white solid, which was analyzed by NMR spectroscopy. ^{1}H NMR of **2** (400 MHz, $CDCl_3$, 25°C): $\delta = 5.95$ (br m, 3H; $-CH{=}CH_2$ and $-CH{=}CH_2$), 4.20 (br s, 1H; −OCH−),1.85 (m, 6H; −CH−),1.23 (m, 6H; $-OCH-(CH_3)_2$),0.96 (m, 36H; $-CH_3$), 0.60 ppm (m, 12H; $-CH_2-$).

Synthesis of the hybrid material PS-TiPOSS/SBA-15: Mesoporous silica support SBA-15 was synthesized according a reported procedure.[25] Styrene (Merck, 99%) and divinylbenzene (Aldrich, 80%, mixture of isomers) were purified before use with an alumina column to remove the polymerization inhibitor. In a typical synthesis of the PS-TiPOSS/SBA-15 hybrid material, SBA-15 (0.5 g, degassed overnight at 350°C) was impregnated with a solution of comonomers (0.13 g, molar ratio styrene/divinylbenzene = 8:2), benzoyl peroxide (0.018 g; Aldrich, 97%) and Vi-TiPOSS (**2**) (0.075 g) in CH_2Cl_2 (1.5 mL). After impregnation for 2 h, the solvent was slowly removed at 40°C to achieve a uniform distribution of monomers.[21] The material was subjected to freeze–pump–thaw cycles and sealed under vacuum. Polymerization was performed at 60°C for 4 h, and continued at 100°C for 10 h. The recovered material was washed thoroughly with chloroform and dried under vacuum. Samples thus obtained were denoted PS*x*-TP*y*, as explained under the Results and Discussion section.

Characterization: MALDI-TOF-MS analysis was performed using a Voyager-De STR instrument. X-ray diffraction (XRD) data were collected on a Bruker-D8 Advance X-ray diffractometer with $Cu_{K\alpha}$ radiation with the capillary model, operated at 40 kV and 30 mA. The nitrogen sorption was measured on a Tristar 3000 Micromeritics apparatus that allowed the analysis of up to three solids at one time. For sample preparation a Micromeritics Smartprep apparatus was used to treat the samples at 150°C under a nitrogen flow for 5 h. SEM measurements were performed using a Philips environmental scanning electron microscope XL-30 ESEM FEG (Philips, The Netherlands; now Fei Co.) in high-vacuum mode with acceleration voltages of 2 kV (low-voltage SEM, LVSEM) and a secondary electron (SE) detector. TEM was performed using a Philips CM30T electron microscope with an LaB6 filament as the source of electrons, operated at 300 kV. ^{29}Si and ^{13}C CP-MAS NMR spectra were recorded on a Bruker DMX500 spectrometer. Infrared spectra were recorded on a Nicolet Avatar 360 spectrometer with a KBr pellet. Inductively coupled plasma optical emission spectrometry (ICP-OES) was used to determine the titanium content in the hybrid materials. The measurements were performed with a Spectro CIROSCCD spectrometer equipped with a free-running 27.12 MHz generator at 1400 W. Thermal gravimetric analysis (TGA) was performed on a Netzsch TG 2097-1 Iris instrument under an oxygen atmosphere. Catalyst screening was performed on a Chemspeed ASW 1000 workstation equipped with 10 mL reactors.

Epoxidations with TBHP as the oxidant: Cyclooctene (5.0 M in isooctane), TBHP (2.0 M in isooctane), catalyst, and 1,3,5-trimethylbenzene (Acros, 99%) as GC internal standard were transferred into the reaction vessels, resulting in reaction mixtures (each 1.40 mL) with [TBHP] = [cyclooctene] = 1.29 M, [Ti] = 0.005 M. The reaction was performed at 60°C for 17 h.

For the kinetic investigation, a different protocol was applied: cyclooctene (5.0 M in isooctane), TBHP (2.0 M in isooctane), catalyst (in isooctane) and 1,3,5-trimethylbenzene (TMB) were transferred into the reaction vessels, resulting in reaction mixtures (each 2.25 mL) with [TBHP] = [cyclooctene] = 1 M, [Ti] = 0.001 M. The reaction was performed at 60°C. At suitable time intervals, samples (0.1 mL) were taken from the reactors, filtered through syringe filters (0.45 μm), injected into GC vials containing MeOH (0.9 mL), and analyzed by GC.

Epoxidations with aqueous H_2O_2: H_2O_2 (35% aqueous solution; Acros), catalyst, and neat alkene were mixed together in the reaction vessels (molar ratios cyclooctene/H_2O_2 = 4:1, H_2O_2/Ti = 250:1). TMB was added as the internal standard. The reaction was performed at 60°C for 17 h.

Recycling tests on the hybrid catalysts: Before each cycle, the catalyst was washed with chloroform three times and dried under vacuum. In the recycling reactions, the weight ratios of the catalyst, reactant, and oxidant were kept constant.

Acknowledgements

This work was supported financially by the Programme for Strategic Scientific Alliances between China and the Netherlands (PSA), 04-PSA-M-01 and NSFC 20321303. We thank M. A. van Straten (TU/e) for the MALDI-TOF-MS analyses and A. Elemans-Mehring (TU/e) for assisting with the ICP measurements.

[1] M. G. Voronkov, V. I. Lavrent'yev, *Top. Curr. Chem.* **1982**, *102*, 199–236.
[2] P. G. Harrison, *J. Organomet. Chem.* **1997**, *542*, 141–183.
[3] H. C. L. Abbenhuis, *Chem. Eur. J.* **2000**, *6*, 25–32.
[4] F. J. Feher, T. A. Budzichowski, *Polyhedron* **1995**, *14*, 3239–3253.
[5] R. W. J. M. Hanssen, R. A. van Santen, H. C. L. Abbenhuis, *Eur. J. Inorg. Chem.* **2004**, *4*, 675–683.
[6] R. Duchateau, *Chem. Rev.* **2002**, *102*, 3525–3542.
[7] H. C. L. Abbenhuis, S. Krijnen, R. A. van Santen, *Chem. Commun.* **1997**, 331–332.
[8] T. Maschmeyer, M. Klunduk, C. C. M. Martin, D. S. Shephard, J. M. Thomas, B. F. G. Johnson, *Chem. Commun.* **1997**, 1847–1848.
[9] M. Crocker, R. H. M. Herold, A. G. Orpen, M. T. A. Overgaag, *J. Chem. Soc. Dalton Trans.* **1999**, *21*, 3791–3804.
[10] P. P. Pescarmona, J. C. van der Waal, I. E. Maxwell, T. Maschmeyer, *Angew. Chem.* **2001**, *113*, 762–765; *Angew. Chem. Int. Ed.* **2001**, *40*, 740–743.

[11] M. L. W. Vorstenbosch, A. L. Spek, H. Kooijman, M. Lutz, G. Gerritsen, N. Ní Bhriain, R. M. Paulus, M. W. M. Fijten, R. Hoogenboom, U. Schubert, R. A. van Santen, D. Vogt, H. C. L. Abbenhuis, unpublished results.
[12] S. Krijnen, H. C. L. Abbenhuis, R. W. J. M. Hanssen, J. H. C. van Hooff, R. A. van Santen, *Angew. Chem.* **1998**, *110*, 374–376; *Angew. Chem. Int. Ed.* **1998**, *37*, 356–358.
[13] S. Krijnen, B. L. Mojet, H. C. L. Abbenhuis, J. H. C. van Hooff, R. A. van Santen, *Phys. Chem. Chem. Phys.* **1999**, *1*, 361–365.
[14] M. D. Skowronska-Ptaskinska, M. L. W. Vorstenbosch, R. A. van Santen, H. C. L. Abbenhuis, *Angew. Chem.* **2002**, *114*, 659–661; *Angew. Chem. Int. Ed.* **2002**, *41*, 637–639.
[15] For recent reviews on immobilization of homogeneous catalysts, please see: a) N. E. Leadbeater, M. Marco, *Chem. Rev.* **2002**, *102*, 3217–3274; b) C. A. McNamara, M. J. Dixon, M. Bradley, *Chem. Rev.* **2002**, *102*, 3275–3300; c) Q. H. Fan, Y. M. Li, A. S. C. Chan, *Chem. Rev.* **2002**, *102*, 3385–3466; d) C. E. Song, S. Lee, *Chem. Rev.* **2002**, *102*, 3495–3524; e) D. E. De Vos, M. Dams, B. F. Sels, P. A. Jacobs, *Chem. Rev.* **2002**, *102*, 3615–3640; f) P. Mastrorilli, C. F. Nobile, *Coord. Chem. Rev.* **2004**, *248*, 377–395.
[16] K. Moller, T. Bein, *Chem. Mater.* **1998**, *10*, 2950–2963.
[17] C. G. Wu, T. Bein, *Science* **1994**, *264*, 1757–1759.
[18] K. Moller, T. Bein, R. X. Fischer, *Chem. Mater.* **1999**, *11*, 665–673.
[19] K. Moller, T. Bein, R. X. Fischer, *Chem. Mater.* **1998**, *10*, 1841–1852.
[20] T. Q. Nguyen, J. J. Wu, V. Doan, B. J. Schwartz, S. H. Tolbert, *Science* **2000**, *288*, 652–656.
[21] M. Choi, F. Kleitz, D. Liu, H. Y. Lee, W. S. Ahn, R. Ryoo, *J. Am. Chem. Soc.* **2005**, *127*, 1924–1932.
[22] D. Zhao, J. Feng, Q. Huo, N. Melosh, G. H. Fredrickson, B. F. Chmelka, G. D. Stucky, *Science* **1998**, *279*, 548–552.
[23] H. J. Shin, R. Ryoo, M. Kruk, M. Jaroniec, *Chem. Commun.* **2001**, 349–350.
[24] S. Jun, S. H. Joo, R. Ryoo, M. Kruk, M. Jaroniec, Z. Liu, T. Ohsuna, O. Terasaki, *J. Am. Chem. Soc.* **2000**, *122*, 10712–10713.
[25] M. Choi, W. Heo, F. Kleitz, R. Ryoo, *Chem. Commun.* **2003**, 1340–1341.
[26] M. Choi, R. Ryoo, *Nat. Mater.* **2003**, *2*, 473–476.
[27] A. Dubey, M. Choi, R. Ryoo, *Green Chem.* **2006**, *8*, 144–146.
[28] A. Sayari, S. Hamoudi, *Chem. Mater.* **2001**, *13*, 3151–3168.
[29] F. Kleitz, W. Schmidt, F. Schuth, *Microporous Mesoporous Mater.* **2003**, *65*, 1–29.
[30] E. P. Barrett, L. G. Joyner, P. P. Halenda, *J. Am. Chem. Soc.* **1951**, *73*, 373–380.
[31] M. Kruk, M. Jaroniec, S. H. Joo, R. Ryoo, *J. Phys. Chem. B* **2003**, *107*, 2205–2213.
[32] P. Van Der Voort, P. I. Ravikovitch, K. P. De Jong, M. Benjelloun, E. Van Bavel, A. H. Janssen, A. V. Neimark, B. M. Weckhuysen, E. F. Vansant, *J. Phys. Chem. B* **2002**, *106*, 5873–5877.
[33] B. C. Lippens, J. H. De Boer, *J. Catal.* **1965**, *4*, 319–323.
[34] P. Meenakshi, S. E. Noorjahan, R. Rajini, U. Venkateswarlu, C. Rose, T. P. Sastry, *Bull. Mater. Sci.* **2002**, *25*, 25–29.
[35] A. Mercier, K. Kuroki, I. Ando, H. Deleuze, O. Mondain-Monval, *J. Polym. Sci. Part B* **2001**, *39*, 956–963.
[36] C. Li, *J. Catal.* **2003**, *216*, 203–212.
[37] a) C. Li, G. Xiong, Q. Xin, J. K. Liu, P. L. Ying, Z. Feng, J. Li, W. B. Yang, Y. Z. Wang, G. R. Wang, X. Y. Liu, M. Lin, X. Q. Wang, E. Z. Min, *Angew. Chem.* **1999**, *111*, 2358–2360; *Angew. Chem. Int. Ed.* **1999**, *38*, 2220–2222; b) C. Li, G. Xiong, J. Liu, P. Ying, Q. Xin, Z. Feng, *J. Phys. Chem. B* **2001**, *105*, 2993–2997.
[38] a) J. Q. Yu, Z. C. Feng, L. Xu, M. J. Li, Q. Xin, Z. M. Li, *Chem. Mater.* **2001**, *13*, 994–998; b) W. H. Zhang, J. Lu, B. Han, M. Li, J. Xiu, P. Ying, C. Li, *Chem. Mater.* **2002**, *14*, 3413–3421.
[39] Q. Yang, S. Wang, J. Lu, G. Xiong, C. Li, *Appl. Catal. A* **2000**, *194*, 507–514.

Received: May 30, 2006
Published online: October 25, 2006

